

Cu Nanowire@Microporous Organic Polymer with Hydroquinones: Pseudocapacitive Materials with High Rate Performance

Jin Hwan Jung,[†] Chang Wan Kang,[†] and Seung Uk Son^{*}Cite This: *ACS Appl. Energy Mater.* 2022, 5, 13149–13154

Read Online

ACCESS |



Metrics & More



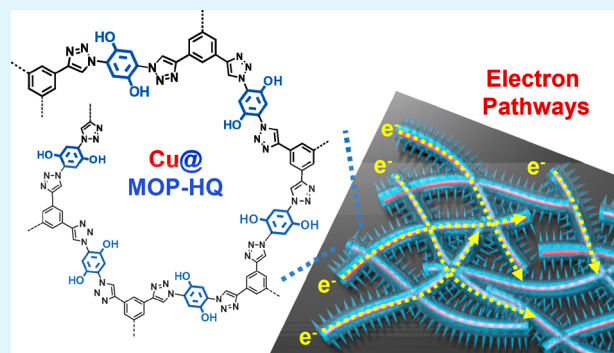
Article Recommendations



Supporting Information

ABSTRACT: Microporous organic polymers with redox-active hydroquinones (MOP-HQs) were synthesized on Cu nanowires through the surface Cu₂O-catalyzed azide–alkyne click reaction. The resultant Cu@MOP-HQ2 with the optimized contents of MOP-HQ and Cu nanowires showed high capacitances up to 370 F/g (@0.5 A/g) and 360 F/g (@1 A/g), respectively, for pseudocapacitors. In particular, the Cu@MOP-HQ2 retained capacitances of 348 and 343 F/g at high current densities of 10 and 20 A/g, respectively. During 10000 cycling tests, coin cell-type pseudocapacitors maintained 98.3–98.6% of their original capacitances. The excellent electrochemical performance of Cu@MOP-HQ2 is attributable to an electron pathway role of incorporated Cu nanowires.

KEYWORDS: microporous organic polymer, pseudocapacitor, energy storage material, hydroquinone, copper nanowire



Microporous organic polymers (MOPs) are versatile materials for various applications such as adsorbents, catalysis, and biomedical therapy.¹ In addition, MOPs have been recently applied to various energy issues.^{1–3} For example, it has been demonstrated that the MOPs are highly promising as electrical energy storage materials, due to high surface areas, porosity, stability, and chemical tunability.^{2,3}

As human society continues to be modernized, the utilization of electrical energy is diversified. In this regard, electrical energy storage is becoming an increasingly important issue. Supercapacitors and batteries are recognized as main electrical energy storage devices.^{4–6} While supercapacitors have advantages over redox-based batteries in terms of fast power generation, their relatively low energy storage capacity is a critical drawback.^{4–6} Thus, the introduction of redox-active species into capacitive materials is an efficient strategy for improving their energy storage capacities, generating so-called pseudocapacitors.⁷ In this regard, recently, MOPs bearing redox-active carbazole, triphenylamine, 1,4-dicarbonylbenzene, ferrocene, phenazine, oxadiazoles, etc. have been prepared for the engineering of pseudocapacitors (Table S1 in the SI).^{2,3,8–13} In addition, the chemical conversion between hydroquinones and benzoquinones is one of the representative organic redox systems in the engineering of redox-active MOP materials.¹⁴

However, the low conductivity of MOPs represents the key problem for their application as electrical energy storage materials. To improve the electrochemical performance of MOPs as energy storage materials, further explorations for enhancing their conductivity are required. We think that the

incorporation of conductive materials such as metallic Cu materials into MOPs can be one way to improve conductivity. While carbon nanotubes, graphenes, or carbon nanopowders have recently been incorporated into MOPs to enhance their electrochemical performance (Table S1 in the SI),^{15–18} as far as we are aware, metallic nanowire-based MOP composites have yet to be reported for electrical energy storage materials.

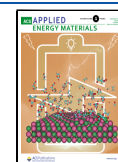
In general, MOPs can be prepared through the networking of organic building blocks.^{1–3} While various transition metal-catalyzed coupling reactions have been used for the preparation of MOPs, the Huisgen azide–alkyne 1,3-dipolar cycloaddition, the so-called click reaction, is also very useful in the synthesis of functional polymers.¹⁹ Recently, various MOPs have been reported by the click reaction of multiethynylarenes and multiazidoarenes.^{20,21} It is known that various Cu(I) species can catalyze the azide–alkyne 1,3-dipolar click reaction.²² For example, Cu₂O powders are known to catalyze the azide–alkyne click reaction.²³

During the past two decades, there has been great progress in the size- and morphology-controlled synthesis of metallic nanomaterials.²⁴ Recently, Cu nanowires have also been prepared through the growth-controlled synthesis.²⁵ It has been known that the surface of Cu nanomaterials consists of

Received: August 22, 2022

Accepted: October 7, 2022

Published: October 18, 2022



air-oxidized Cu_2O layers.²⁶ Thus, we think that the Cu nanowires can be introduced into MOPs through the surface Cu_2O -catalyzed azide–alkyne click reaction of multiethynylarenes and multiazidoarenes. In this work, we report the preparation of Cu nanowire@MOP with hydroquinones (Cu@MOP-HQs) and their electrochemical performance as pseudocapacitive materials.

Figure 1 shows a synthetic scheme of Cu@MOP-HQs . First, Cu nanowires were prepared by the synthetic procedures

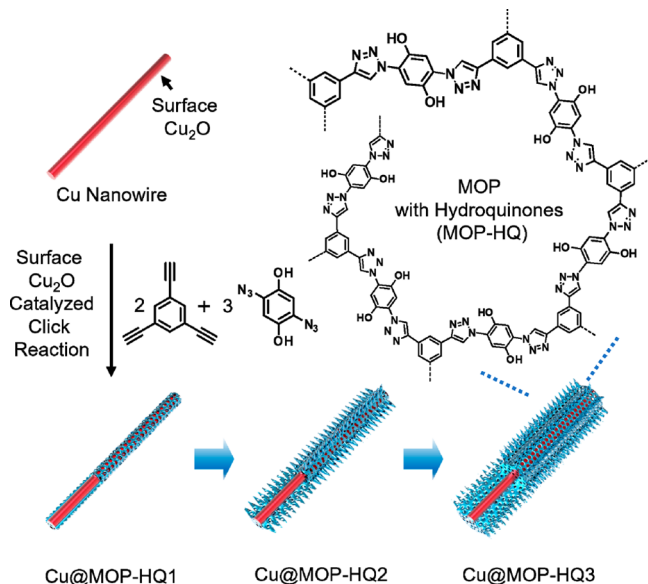


Figure 1. Synthesis of Cu nanowire@microporous organic polymer with hydroquinones (Cu@MOP-HQs).

reported in the literature.²⁵ The azide–alkyne click reaction of 1,3,5-triethynylbenzene with 1,4-diazido-2,5-dihydroxybenzene in the presence of Cu nanowires generated MOPs on the surface of Cu nanowires. Considering the Cu(I) species-catalyzed azide–alkyne click reaction,^{22,23} we think that the Cu_2O on the surface of Cu nanowires catalyzed the click reaction of organic building blocks. With a fixed amount of Cu nanowires (10 mg), we gradually increased the amount of 1,3,5-triethynylbenzene from 8.3 μmol to 17 and 33 μmol with 1.5 equiv of 1,4-diazido-2,5-dihydroxybenzene, generating three Cu@MOP-HQs that were denoted as Cu@MOP-HQ1 , Cu@MOP-HQ2 , and Cu@MOP-HQ3 , respectively.

The morphologies of Cu nanowires and Cu@MOP-HQs were investigated by scanning (SEM) and transmission (TEM) electron microscopy (Figure 2). As shown in Figures 2a,b, the prepared Cu nanowires had a length of 3–5 μm and a thickness of 20–30 nm. High-resolution (HR) TEM analysis showed thin Cu_2O layers with a thickness of ~ 3.5 nm on the surface of Cu nanowires (Figure 2c). In addition, the (111) crystal planes of Cu_2O layers and Cu were mainly observed with the interplane distances of 0.25 and 0.21 nm, respectively (Figure 2c).

The SEM images of Cu@MOP-HQs showed that the Cu nanowires were homogeneously coated with MOP materials (Figures 2d–f). The diameters of Cu@MOP-HQs gradually increased from 80–115 nm (Cu@MOP-HQ1) to 200–240 nm (Cu@MOP-HQ2) and 300–350 nm (Cu@MOP-HQ3). TEM analysis showed that, after the Cu nanowires were coated with the relatively dense MOPs in Cu@MOP-HQ1 , the 2D

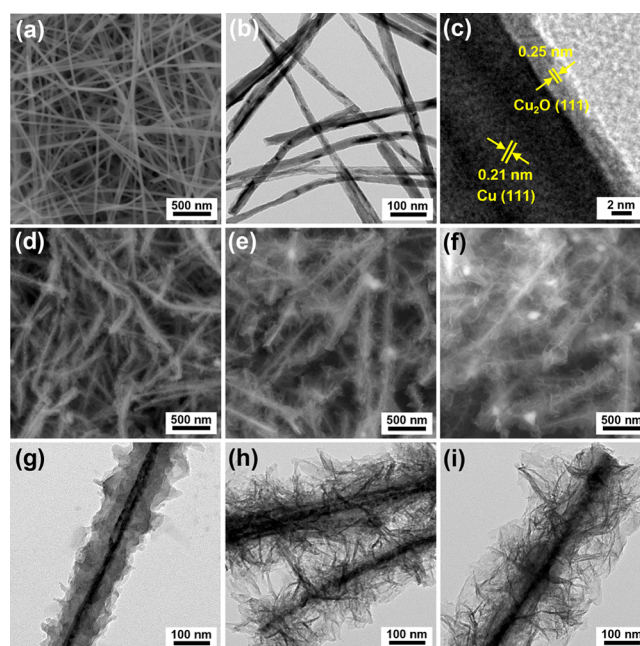


Figure 2. SEM images of (a) Cu nanowires, (d) Cu@MOP-HQ1 , (e) Cu@MOP-HQ2 , and (f) Cu@MOP-HQ3 . TEM images of (b) Cu nanowires, (g) Cu@MOP-HQ1 , (h) Cu@MOP-HQ2 , and (i) Cu@MOP-HQ3 . (c) A HR-TEM image of Cu nanowires.

MOP plates were formed in Cu@MOP-HQ2 and Cu@MOP-HQ3 (Figures 2g–i). The SEM and TEM images showed the existence of Cu nanowires with a thickness of 20–30 nm at the center of Cu@MOP-HQs (Figures 2d–i).

Powder X-ray diffraction (PXRD) studies indicated that Cu nanowires consist of metallic Cu with a small amount of Cu_2O . The PXRD pattern of Cu nanowires showed diffraction peaks at the 2θ values of 43.1°, 50.3°, and 74.0°, corresponding to the (111), (200), and (220) crystalline planes of face-centered cubic Cu (JCPDS 01-1241), respectively, in addition to trace peaks at the 2θ values of 36.4°, 42.3°, and 61.6°, corresponding to the (111), (200), and (220) crystalline planes of Cu_2O (JCPDS 05-0667), respectively (Figure 3a).²⁶ The PXRD patterns of Cu@MOP-HQs indicated the existence of major metallic Cu and minor Cu_2O (Figure 3a). As the amount of MOP-HQ in Cu@MOP-HQs increased, the relative intensity of Cu_2O to that of Cu decreased, due to the increased consumption of Cu_2O species in the azide–alkyne click reaction-based formation of MOPs. The X-ray photoelectron spectrum (XPS) of Cu nanowires showed Cu $2p_{1/2}$ and $2p_{3/2}$ orbital peaks at 952.1 and 932.1 eV, respectively, corresponding to the zerovalent Cu species (Figure 3b).²⁷ The Cu $2p_{1/2}$ and $2p_{3/2}$ orbital peaks of Cu@MOP-HQs were slightly shifted to 952.4 and 932.4 eV, respectively, indicating the electronic interaction of Cu nanowires with MOP-HQs.

The surface areas and porosity of Cu@MOP-HQ were investigated through the analysis of N_2 adsorption–desorption isotherm curves obtained at 77 K (Figures 3c,d). While the Cu nanowires showed a low surface area of 10 m^2/g with nonporosity, Cu@MOP-HQs showed enhanced surface areas and porosity. As the amount of MOP-HQs in Cu@MOP-HQs increased, the surface areas gradually increased from 146 m^2/g (Cu@MOP-HQ1) to 223 m^2/g (Cu@MOP-HQ2) and 342 m^2/g (Cu@MOP-HQ3), respectively, with increased micro/

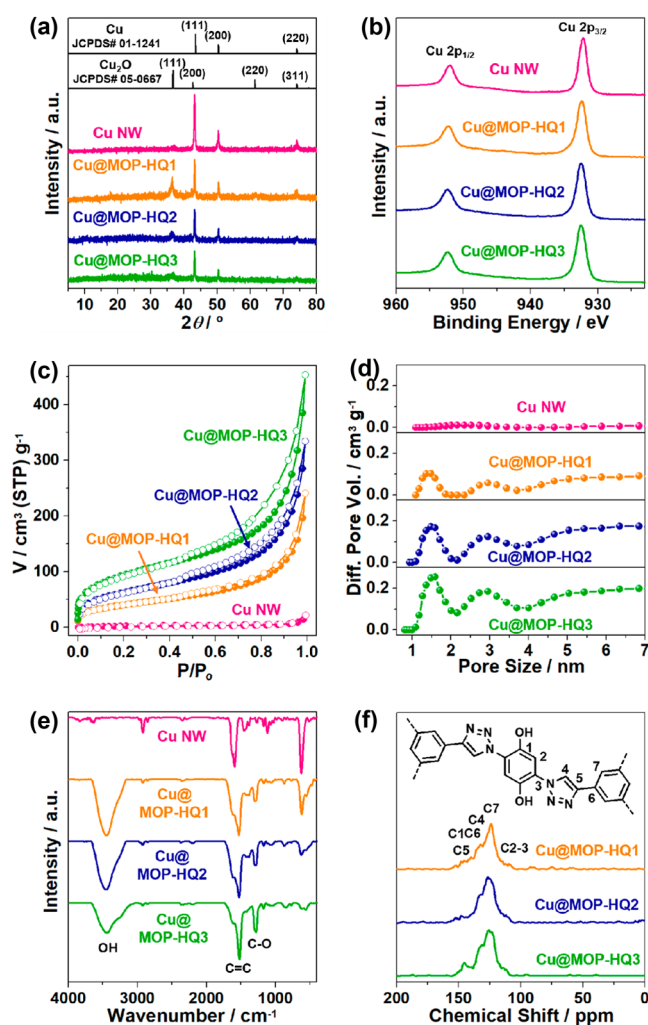


Figure 3. (a) PXRD patterns, (b) XPS Cu 2p orbital spectra, (c) N_2 adsorption–desorption isotherm curves obtained at 77 K, (d) pore size distribution diagrams based on the DFT method, and (e) IR spectra of Cu nanowires, Cu@MOP-HQ1, Cu@MOP-HQ2, and Cu@MOP-HQ3. (f) Solid state CP/TOSS ^{13}C NMR spectra of Cu@MOP-HQ1, Cu@MOP-HQ2, and Cu@MOP-HQ3.

mesoporosity (Figures 3c,d), indicating the successful formation of MOPs.

The chemical structures of MOP-HQs in Cu@MOP-HQs were further characterized by infrared (IR) and solid state ^{13}C nuclear magnetic resonance (NMR) studies (Figures 3e,f). In the IR spectra of Cu@MOP-HQs, aromatic C=C, C–O, and O–H vibration peaks were, respectively, observed at 1520, 1283, and 3444 cm^{-1} , matching those of hydroquinone moieties in the literature (Figure 3e).²⁸ The solid state ^{13}C NMR spectra of Cu@MOP-HQs showed significantly overlapped aromatic ^{13}C peaks at 107–155 ppm, in addition to the ^{13}C peaks of triazole rings at 145 ppm (Figure 3f), indicating that the MOP-HQs were formed by the azide–alkyne click reaction between organic building blocks. According to the combustion elemental analysis of nitrogens, the contents of hydroquinones in Cu@MOP-HQ1, Cu@MOP-HQ2, and Cu@MOP-HQ3 were measured to be 0.33, 0.45, and 0.69 mmol/g, respectively. The thermogravimetric analysis (TGA) showed that Cu@MOP-HQs are thermally stable up to 262 °C (Figure S1 in the SI).

Considering the conjugated structure, redox-active hydroquinones, and incorporated Cu nanowires of Cu@MOP-HQs, their electrochemical performance as electrode materials for symmetric coin cell-type pseudocapacitors were studied.²⁹ Figures 4–7 summarize the results.

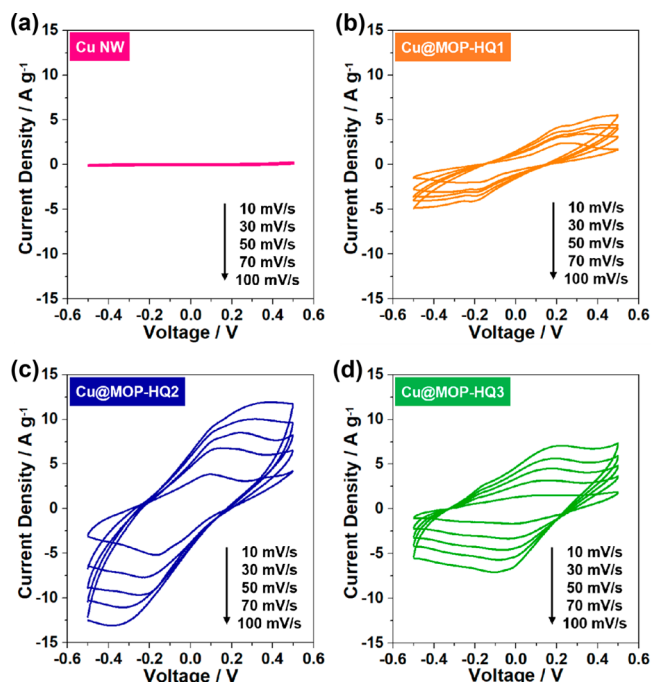


Figure 4. Scan rate-dependent cyclic voltammograms of (a) Cu nanowires, (b) Cu@MOP-HQ1, (c) Cu@MOP-HQ2, and (d) Cu@MOP-HQ3 in 1 M H_2SO_4 electrolyte.

At first, the electrochemical responses of Cu nanowires and Cu@MOP-HQs were investigated in 1 M H_2SO_4 electrolyte by cyclic voltammetry (Figure 4). While Cu nanowires showed relatively poor capacitive behavior in the scan rate-dependent cyclic voltammograms (Figure 4a), Cu@MOP-HQ1 showed enhanced capacitive and redox responses (Figure 4b). Compared with Cu@MOP-HQ1, the electrochemical response of Cu@MOP-HQ2 was significantly enhanced with redox peaks at 0.12–0.23 V, due to the increased amount of pseudocapacitive MOP-HQs (Figure 4c). In comparison, the electrochemical response of Cu@MOP-HQ3 was reduced, compared with that of Cu@MOP-HQ2, possibly due to the decreased conductivity (Figure 4d). Thus, the observed order of electrochemical performance was Cu@MOP-HQ2 > Cu@MOP-HQ3 > Cu@MOP-HQ1. These observations indicate that the optimal amount of pseudocapacitive MOP-HQs and conductive Cu nanowires is critical for achieving the best electrochemical performance.

The electrochemical processes of Cu@MOP-HQs were investigated in further detail by analyzing the scan rate-dependent cyclic voltammograms based on the following equation: $i_p = av^b$ (i_p , peak currents; v , scan rates; a and b , variable parameters) (Figure 5a and Figure S2 in the SI).³⁰ In this analysis, while $b = 1$ indicates a capacitive process, $b = 0.5$ implies a redox process.³⁰ As analyzed in Figure 5a, the b values of Cu@MOP-HQ2 were 0.65–0.74, indicating that its electrochemical process consists of both redox and capacitive behaviors. As the amount of MOP-HQ in Cu@MOP-HQs increased, the b values gradually increased from 0.56–0.66

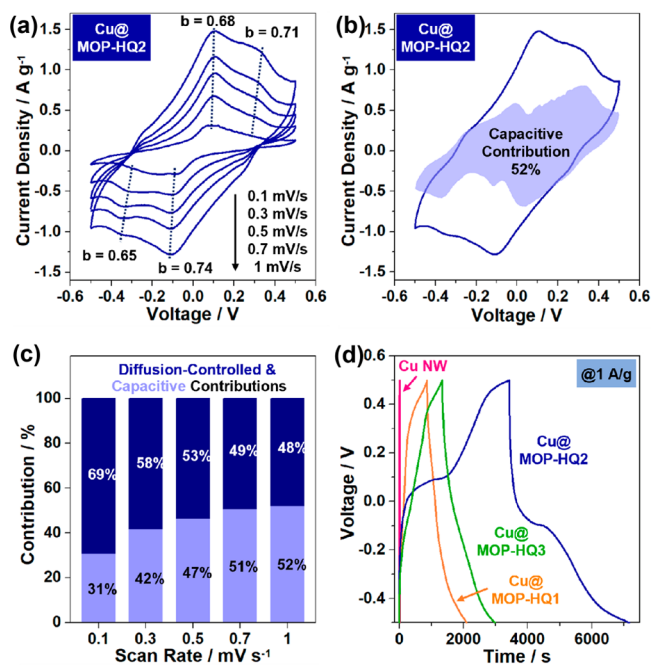


Figure 5. (a) Analysis of scan rate-dependent cyclic voltammograms based on the equation $i_p = a\nu^b$ (i_p , peak currents; ν , scan rates; a and b , variable parameters) and (b, c) the contributions of diffusion-controlled and capacitive processes of Cu@MOP-HQ2 (refer to Figure S2 in the SI for the cyclic voltammogram analysis of other Cu@MOP-HQs). (d) Charge–discharge profiles (current density: 1 A/g) of Cu nanowires, Cu@MOP-HQ1, Cu@MOP-HQ2, and Cu@MOP-HQ3 (refer to Figure S3 in the SI for the current density-dependent charge–discharge profiles of Cu@MOP-HQs).

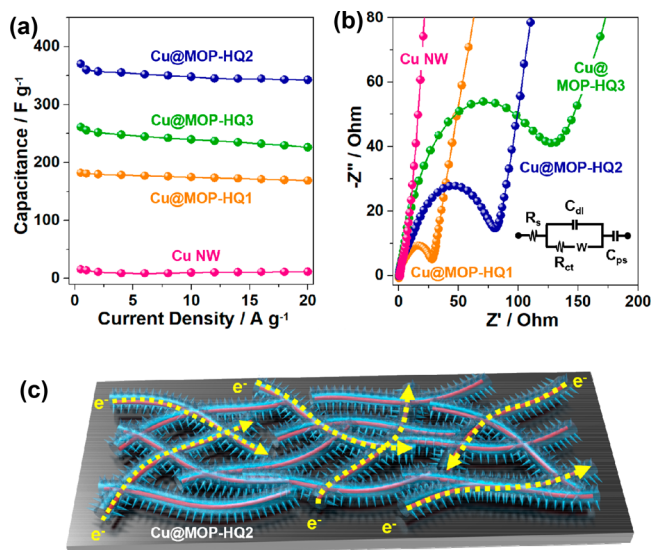


Figure 6. (a) Current density-dependent rate performance and (b) Nyquist plots with a simulated circuit of Cu nanowires, Cu@MOP-HQ1, Cu@MOP-HQ2, and Cu@MOP-HQ3 (refer to Figure S4 in the SI for the detailed analysis of the Nyquist plots). (c) Illustration of electron pathways through the core Cu nanowires of Cu@MOP-HQ2 on a current collector.

(Cu@MOP-HQ1) to 0.73–0.82 (Cu@MOP-HQ3), indicating the increased capacitive process (Figure S2 in the SI). The contributions of capacitive and redox processes were further analyzed by the following equation: $i = k_1\nu + k_2\nu^{1/2}$ (i , current;

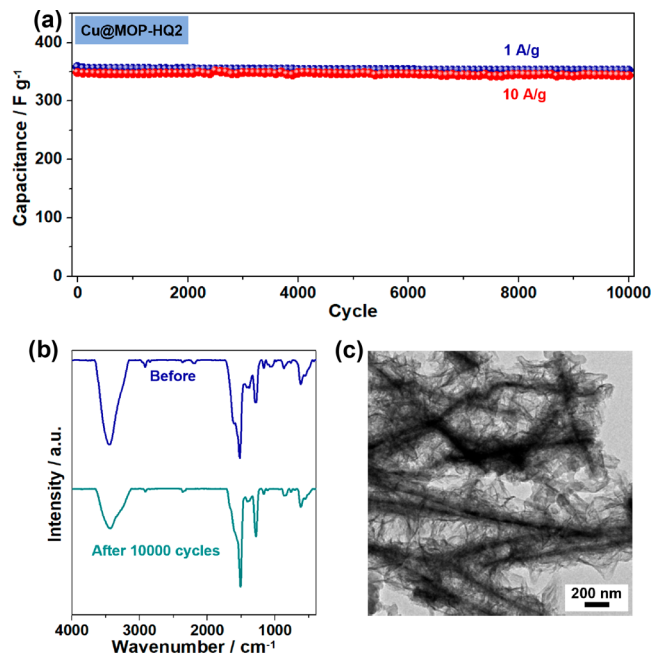


Figure 7. (a) Cycling performance of Cu@MOP-HQ2 at current densities of 1 and 10 A/g. (b) IR and (c) TEM analysis of Cu@MOP-HQ2 retrieved after 10000 cycles.

$k_1\nu$, capacitive process; $k_2\nu^{1/2}$, redox process) (Figure 5c and Figure S2 in the SI).³⁰ As the scan rates increased from 0.1 mV/s to 1 mV/s, the capacitive contributions of Cu@MOP-HQ2 increased gradually from 31% to 52%. As the amount of MOP-HQ in Cu@MOP-HQs increased, the capacitive contributions at a scan rate of 1 mV/s gradually increased from 30% (Cu@MOP-HQ1) to 52% (Cu@MOP-HQ2) and 75% (Cu@MOP-HQ3), matching the observed trend of b values (Figure S2 in the SI).

The charge–discharge (CD) profiles of Cu nanowires and Cu@MOP-HQs were investigated in the voltage range from +0.5 to −0.5 V (Figure 5d and Figure S3 in the SI), showing the pseudocapacitive behavior of Cu@MOP-HQs. As observed in the cyclic voltammograms, the Cu@MOP-HQ2 showed the best electrochemical performance with enhanced capacitive and redox behaviors (Figures 4 and 5d).

The Cu@MOP-HQs showed excellent rate performance, due to the existence of conductive Cu nanowires (Figure 6a). The capacitances of Cu nanowires, Cu@MOP-HQ1, Cu@MOP-HQ2, and Cu@MOP-HQ3, were measured to be 16, 182, 370, and 261 F/g, respectively, at the current density of 0.5 A/g, matching the observed trend of electrochemical responses in the cyclic voltammograms and CD profiles. When the current density increased to 1 and 2 A/g, the capacitances of Cu@MOP-HQ2 were retained with 360 and 357 F/g, respectively. Even when the current density increased to 10 and 20 A/g, the capacitances of Cu@MOP-HQ2 were significantly retained with 348 and 343 F/g, respectively.

Electrochemical impedance spectroscopy (EIS) was conducted to characterize the resistances of the fabricated electrode materials (Figure 6b and Figure S4 in the SI). While the charge transfer resistance (R_{ct}) of the electrode materials containing Cu nanowires was measured to be 12.4 Ω , those of Cu@MOP-HQs gradually increased to 23.8 Ω (Cu@MOP-HQ1), 70.4 Ω (Cu@MOP-HQ2), and 107 Ω (Cu@MOP-HQ3) with the increased amount of MOP-HQs (Figure

S4 in the SI). The conductivities of Cu nanowires and Cu@MOP-HQs were characterized through the measurement of sheet resistances by a four probe method (Figure S5 in the SI). The sheet resistances of Cu nanowires, Cu@MOP-HQ1, Cu@MOP-HQ2, and Cu@MOP-HQ3 were measured to be 0.14, 0.49, 0.89, and 1.97 Ω/sq , respectively, corresponding to the conductivities of 4.8×10^4 , 1.2×10^4 , 5.4×10^3 , and 3.4×10^3 S/m, respectively. As illustrated in Figure 6c, the enhanced electrochemical performance of Cu@MOP-HQ2 is attributable to the inner Cu nanowires that serve as electron pathways on current collectors.

The charge–discharge cycling performance of Cu@MOP-HQ2 was investigated for 10000 cycles (Figure 7a and Figure S6 in the SI). When the symmetric coin cell-type pseudocapacitors fabricated with Cu@MOP-HQ2 were operated for 10000 charge–discharge cycles at the current densities of 1 and 10 A/g, they showed the 98.3% (352 F/g) and 98.6% (344 F/g) retention of the original capacitances (358 and 349 F/g) of the first cycles, respectively. The Cu@MOP-HQ2 retrieved after 10000 charge–discharge cycles was investigated by IR and TEM studies, showing that its original chemical structure and morphology were completely retained (Figures 7b,c).

When the electrochemical studies of Cu@MOP-HQ2 were conducted in KOH electrolyte, instead of H_2SO_4 electrolyte, its electrochemical responses became quite poor (Figure S7 in the SI). It can be speculated that the existence of protons in electrolyte is beneficial in the redox-induced chemical conversion between hydroquinone and benzoquinone species of Cu@MOP-HQ2. To directly compare the electrochemical properties of Cu@MOP-HQ2 with those of the control MOP-HQ2 material, we tried to etch core Cu nanowires from Cu@MOP-HQ2 with a commercial Cu etchant (FeCl_3 -based oxidizing solution). However, unfortunately, the resultant MOP-HQ2 was gradually decomposed through chemical oxidation by the Cu etchant. Thus, alternative control MOP-HQ material was prepared using an excess amount of organic building blocks, 1,3,5-triethynylbenzene and 1,4-diazido-2,5-dihydroxybenzene. As expected, the control MOP-HQ material showed significantly poor electrochemical behavior, due to its poor conductivity (Figures S5 and S7 in the SI).

The electrochemical performance of Cu@MOP-HQ2 was compared with those of MOP-based materials for supercapacitors or pseudocapacitors in the literature (Table S1 in the SI).^{8–13,15–18} First, various redox-active MOPs bearing triazatruxene, anthraquinone, triphenylamine, and 1,4-dicarbonylbenzene moieties have recently been reported in the literature, showing the improved capacitances of 168–193 F/g (@1 A/g), compared with those of control MOPs (Table S1 in the SI). Second, carbon-based conductive materials such as carbon nanotubes, reduced graphene oxides, and carbon black powders have been incorporated into redox-active MOPs, further enhancing the capacitances up to 373 F/g (@1 A/g).^{15–18} Although the rate performance was significantly improved by the incorporation of conductive carbon materials, the redox-active MOPs with carbon black powders showed the retention of capacitances of 280 and 250 F/g at the current densities of 10 and 20 A/g, respectively.^{15–18} In comparison, while the Cu@MOP-HQ2 in this work showed the capacitance of 360 F/g (@1 A/g), it retained the capacitances of 348 and 343 F/g at the current densities of 10 and 20 A/g, respectively. These results indicate that the incorporation of Cu nanowires into the MOPs can be a more efficient strategy for enhancing

rate performance than the incorporation of carbon-based materials. It is noteworthy that while the optimized carbon black nanoparticle@MOPs in the literature showed conductivity of 1.9×10^2 S/m,¹⁷ the Cu@MOP-HQ2 in this work showed the much improved conductivity of 5.4×10^3 S/m.

In conclusion, this work introduces a new strategy for enhancing the electrochemical performance of MOP-based electrical energy storage materials. While MOPs hold considerable potential as electrical energy storage materials, their poor conductivities represent a main obstacle. This work shows that the incorporation of conductive Cu nanowires into the MOP can significantly enhance the electrochemical performance. The surface of Cu nanowires consists of air-oxidized Cu_2O layers. Based on the Cu_2O -catalyzed azide–alkyne click reaction, the MOP-HQs could be incorporated into Cu nanowires. The amount of MOP-HQs could be controlled by scanning the amount of organic building blocks.

Cu@MOP-HQ2 with the optimized contents of MOP-HQs and Cu nanowires showed high specific capacitances of 370 F/g (@0.5 A/g) and excellent rate performance, maintaining 348 and 343 F/g at 10 and 20 A/g, respectively. Moreover, Cu@MOP-HQ2 showed excellent cycling performance for 10000 charge–discharge cycles, maintaining 98.3–98.6% of its original capacitances. The high electrochemical performance of Cu@MOP-HQ2 is attributable to its high conductivity of 5.4×10^3 S/m, due to the existence of conductive Cu nanowires. We believe that the strategy used in this work can be applied for the click reaction-based synthesis of various redox-active MOPs on Cu nanowires.

■ ASSOCIATED CONTENT

Supporting Information

The Supporting Information is available free of charge at <https://pubs.acs.org/doi/10.1021/acsaem.2c02701>.

Additional characterization data and electrochemical properties of Cu@MOP-HQs and a comparison table of electrochemical performance (PDF)

■ AUTHOR INFORMATION

Corresponding Author

Seung Uk Son – Department of Chemistry, Sungkyunkwan University, Suwon 16419, Korea; orcid.org/0000-0002-4779-9302; Email: sson@skku.edu

Authors

Jin Hwan Jung – Department of Chemistry, Sungkyunkwan University, Suwon 16419, Korea

Chang Wan Kang – Department of Chemistry, Sungkyunkwan University, Suwon 16419, Korea

Complete contact information is available at: <https://pubs.acs.org/doi/10.1021/acsaem.2c02701>

Author Contributions

[†]J.H.J. and C.W.K. contributed equally to this work.

Notes

The authors declare no competing financial interest.

■ ACKNOWLEDGMENTS

This work was supported by the National Research Foundation of Korea (NRF) grant (2020R1A2C22004310) funded by the Korea government (MSIT).

REFERENCES

- (1) Cho, K.; Kang, C. W.; Ryu, S. H.; Jang, J. Y.; Son, S. U. The Rise of Morphology-Engineered Microporous Organic Polymers (ME-MOPs): Synthesis and Benefits. *J. Mater. Chem. A* **2022**, *10*, 6950–6964.
- (2) Kang, C. W.; Son, S. U. Redox-Active Porous Organic Polymers for Energy Storage. *Bull. Korean Chem. Soc.* **2021**, *42*, 159–167.
- (3) Amin, K.; Ashraf, N.; Mao, L.; Faul, C. F. J.; Wei, Z. Conjugated Microporous Polymers for Energy Storage: Recent Progress and Challenge. *Nano Energy* **2021**, *85*, 105958.
- (4) Zuo, W.; Li, R.; Zhou, C.; Li, Y.; Xia, J.; Liu, J. Battery-Supercapacitor Hybrid Devices: Recent Progress and Future Prospects. *Adv. Sci.* **2017**, *4*, 1600539.
- (5) Wang, K.; Li, Q.; Ren, Z.; Li, C.; Chu, Y.; Wang, Z.; Zhang, M.; Wu, H.; Zhang, Q. 2D Metal-Organic Frameworks (MOFs) for High-Performance BatCap Hybrid Devices. *Small* **2020**, *16*, 2001987.
- (6) Wang, K.; Wang, S.; Liu, J.; Guo, Y.; Mao, F.; Wu, H.; Zhang, Q. Fe-Based Coordination Polymers as Battery-Type Electrode in Semi-Solid-State Battery-Supercapacitor Hybrid Devices. *ACS Appl. Mater. Interfaces* **2021**, *13*, 15315–15323.
- (7) Fleischmann, S.; Mitchell, J. B.; Wang, R.; Zhan, C.; Jiang, D.; Presser, V.; Augustyn, V. Pseudocapacitance: From Fundamental Understanding to High Power Energy Storage Materials. *Chem. Rev.* **2020**, *120*, 6738–6782.
- (8) Zhang, H.; Zhang, Y.; Gu, C.; Ma, Y. Electropolymerized Conjugated Microporous Poly(zinc-porphyrin) Films as Potential Electrode Materials in Supercapacitors. *Adv. Energy Mater.* **2015**, *5*, 1402175.
- (9) Li, X.-C.; Zhang, Y.; Wang, C.-Y.; Wan, Y.; Lai, W.-Y.; Pang, H.; Huang, W. Redox-active Triazatruxene-Based Conjugated Microporous Polymers for High-Performance Supercapacitors. *Chem. Sci.* **2017**, *8*, 2959–2965.
- (10) Choi, J.; Ko, J. H.; Kang, C. W.; Lee, S. M.; Kim, H. J.; Ko, Y.-J.; Yang, M.; Son, S. U. Enhanced Redox Activity of a Hollow Conjugated Microporous Polymer Through the Generation of Carbonyl Groups by Carbonylative Sonogashira Coupling. *J. Mater. Chem. A* **2018**, *6*, 6233–9237.
- (11) Nazeer, A. A.; Husain, A. A.; Samuel, J.; Rajendran, N.; Makhseed, S. Hydroxyl-Functionalized Microporous Polymer for Enhanced CO₂ Uptake and Efficient Supercapacitor Energy Storage. *React. Funct. Polym.* **2020**, *154*, 104670.
- (12) Park, S. Y.; Kang, C. W.; Lee, S. M.; Kim, H. J.; Ko, Y.-J.; Choi, J.; Son, S. U. Nanoparticulate Conjugated Microporous Polymers with Post-Modified Benzils for Enhanced Pseudocapacitor Performance. *Chem.—Eur. J.* **2020**, *26*, 12343–12348.
- (13) Mohamed, M. G.; Chaganti, S. V.; Li, M.-S.; Samy, M. M.; Sharma, S. U.; Lee, J.-T.; Elsayed, M. H.; Chou, H.-H.; Kuo, S.-W. Ultrastable Porous Organic Polymers Containing Thianthrene and Pyrene Units as Organic Electrode Materials for Supercapacitors. *ACS Appl. Energy Mater.* **2022**, *5*, 6442–6452.
- (14) Singh, C.; Paul, A. Immense Microporous Carbon@Hydroquinone Metamorphosed from Nonporous Carbon as a Supercapacitor with Remarkable Energy Density and Cyclic Stability. *ACS Sustainable Chem. Eng.* **2018**, *6*, 11367–11379.
- (15) Yuan, K.; Guo-Wang, P.; Hu, T.; Shi, L.; Zeng, R.; Forster, M.; Pichler, T.; Chen, Y.; Scherf, U. Nanofibrous and Graphene-Templated Conjugated Microporous Polymer Materials for Flexible Chemosensors and Supercapacitors. *Chem. Mater.* **2015**, *27*, 7403–7411.
- (16) Samy, M. M.; Mohamed, M. G.; El-Mahdy, A. F. M.; Mansoure, T. H.; Wu, K. C. -W.; Kuo, S.-W. High-Performance Supercapacitor Electrodes Prepared from Dispersions of Tetrabenzonaphthalene-Based Conjugated Microporous Polymers and Carbon Nanotubes. *ACS Appl. Mater. Interfaces* **2021**, *13*, 51906–51916.
- (17) Kang, C. W.; Ko, Y.-J.; Lee, S. M.; Kim, H. J.; Choi, J.; Son, S. U. Carbon Black Nanoparticle Trapping: a Strategy to Realize the True Energy Storage Potential of Redox-Active Conjugated Microporous Polymers. *J. Mater. Chem. A* **2021**, *9*, 17978–17984.
- (18) Mohamed, M. G.; Samy, M. M.; Mansoure, T. H.; Sharma, S. U.; Tsai, M.-S.; Chen, J.-H.; Lee, J.-T.; Kuo, S.-W. Dispersions of 1,3,4-Oxadiazole-Linked Conjugated Microporous Polymers with Carbon Nanotubes as a High-Performance Electrode for Supercapacitors. *ACS Appl. Energy Mater.* **2022**, *5*, 3677–3688.
- (19) Shi, Y.; Cao, X.; Gao, H. The Use of Azide-Alkyne Click Chemistry in Recent Syntheses and Applications of Polytriazole-Based Nanostructured Polymers. *Nanoscale* **2016**, *8*, 4864–4881.
- (20) Song, C.; Liu, B.; Nie, J.; Ma, C.; Lu, C.; Wang, F.; Yang, G.; Chen, Z. Photocatalytically Active Conjugated Porous Polymers via Click Chemistry for Heterogeneous Dehydrogenation of Hydrazo Aromatics. *ACS Sustainable Chem. Eng.* **2020**, *8*, 14377–14385.
- (21) Gan, S.; Zeng, Y.; Liu, J.; Nie, J.; Lu, C.; Ma, C.; Wang, F.; Yang, G. Click-Based Conjugated Microporous Polymers as Efficient Heterogeneous Photocatalysts for Organic Transformation. *Catal. Sci. Technol.* **2022**, *12*, 1202–1210.
- (22) Haldón, E.; Nicasio, M. C.; Pérez, P. J. Copper-Catalysed Azide-Alkyne Cycloadditions (CuAAC): an Update. *Org. Biomol. Chem.* **2015**, *13*, 9528–9550.
- (23) Cho, K.; Yang, H.-S.; Lee, I.-W.; Lee, S. M.; Kim, H. J.; Son, S. U. Valorization of Click-Based Microporous Organic Polymer: Generation of Mesoionic Carbene-Rh Species for the Stereoselective Synthesis of Poly(arylacetylene)s. *J. Am. Chem. Soc.* **2021**, *143*, 4100–4105.
- (24) Shi, Y.; Lyu, Z.; Zhao, M.; Chen, R.; Nguyen, Q. N.; Xia, Y. Noble-Metal Nanocrystals with Controlled Shapes for Catalytic and Electrocatalytic Applications. *Chem. Rev.* **2021**, *121*, 649–735.
- (25) Kim, D.; Kwon, J.; Jung, J.; Kim, K.; Lee, H.; Yeo, J.; Hong, S.; Han, S.; Ko, S. H. A Transparent and Flexible Capacitive-Force Touch Pad from High-Aspect-Ratio Copper Nanowires with Enhanced Oxidation Resistance for Applications in Wearable Electronics. *Small Methods* **2018**, *2*, 1800077.
- (26) Son, S. U.; Park, I. K.; Park, J.; Hyeon, T. Synthesis of Cu₂O Coated Cu Nanoparticles and Their Successful Applications to Ullmann-Type Amination Coupling Reactions of Aryl Chlorides. *Chem. Commun.* **2004**, 778–779.
- (27) Dabera, G. D. M.R.; Walker, M.; Sanchez, A. M.; Pereira, H. J.; Beanland, R.; Hatton, R. A. Retarding Oxidation of Copper Nanoparticles without Electrical Isolation and the Size Dependence of Work Function. *Nat. Commun.* **2017**, *8*, 1894.
- (28) Zhang, A.; He, J.; Guan, Y.; Li, Z. Y.; Zhang, Y.; Zhu, J. X. Oxidative Polymerization of Hydroquinone Using Deoxycholic Acid Supramolecular Template. *Sci. China Chem.* **2012**, *55*, 830–835.
- (29) Hao, G.-P.; Lu, A.-H.; Dong, W.; Jin, Z.-Y.; Zhang, X.-Q.; Zhang, J.-T.; Li, W.-C. Sandwich-Type Microporous Carbon Nanosheets for Enhanced Supercapacitor Performance. *Adv. Energy Mater.* **2013**, *3*, 1421–1427.
- (30) Li, S.; Liu, Y.; Zhao, X.; Shen, Q.; Zhao, W.; Tan, Q.; Zhang, N.; Li, P.; Jiao, L.; Qu, X. Sandwich-Like Heterostructures of MoS₂/Graphene with Enlarged Interlayer Spacing and Enhanced Hydrophilicity as High-Performance Cathodes for Aqueous Zinc-Ion Batteries. *Adv. Mater.* **2021**, *33*, 2007480.